Physical Basis, Premises, and Self-Consistency Checks of Aerosol Retrievals from TRMM VIRS

ALEXANDER IGNATOV AND LARRY STOWE

Office of Research and Applications, Climate Research and Applications Division, NOAA/NESDIS, Washington, District of Columbia

(Manuscript received 30 September 1999, in final form 24 June 2000)

ABSTRACT

This paper outlines the processing stream for aerosol retrievals over oceans from the visible and infrared scanner [VIRS; a five-channel radiometer similar to the National Oceanic and Atmospheric Administration's Advanced Very High Resolution Radiometer (AVHRR)] aboard the Tropical Rainfall Measuring Mission (TRMM) satellite, launched in November 1997. Emphasis is on 1) the applying the previously developed AVHRR second-generation aerosol retrieval algorithm to VIRS data to derive an aerosol parameter, indicative of particle size; 2) removing the unwanted ''thermal leak'' signal in the 1.61-μm channel; 3) giving examples of the first aerosol retrievals from space at this wavelength; and 4) assessing the accuracy of the retrievals with theoretical error analyses and empirical self- and interconsistency checks. Aerosol optical depths τ_1^A and τ_2^A are retrieved from reflected solar radiances in VIRS channels 1 and 2 centered at wavelengths $\lambda_1 = 0.63$ and $\lambda_2 = 1.61$ μm, using two independent lookup tables. When τ_1^A and τ_2^A exceed a certain threshold $\tau_{\min}^A$ an effective Ångström exponent α related to particle size is derived as $\alpha = -\ln(\tau_1^A/\tau_2^A)/\ln(\lambda_1/\lambda_2)$. Channel 2 is contaminated by a thermal leak, originating from a secondary spectral response peak centered at $\sim$5.2 μm. If uncorrected, it leads to errors in τ_2^A of 100% or more. To minimize this error, nighttime VIRS ''dark'' radiances in channel 2 have been related empirically to radiances in channels 4 and 5 (10.8 and 12 μm, respectively), and view angle through regression analyses. The reflected component in channel-2 daytime measurements is estimated by subtracting the empirically derived thermal component from the total signal and is used in the retrieval of τ_2^A. Theoretical error analysis is used to identify the limitations of the VIRS retrieval algorithm, whereas actual retrievals are preliminarily evaluated using a set of specially developed empirical checks. The checks show, on average, a high degree of self- and interconsistency but also identify problems with the retrievals, the most noteworthy being trends in retrieved optical depths with viewing and illumination angles. These problems will be tackled in the next-generation aerosol retrieval algorithm.

1. Introduction

One of the objectives of the Tropical Rainfall Measuring Mission (TRMM) satellite, launched in November 1997, is the evaluation of radiative fluxes from the Clouds and the Earth's Radiant Energy System (CERES) instrument on board (Wielicki et al. 1996). The effect of aerosols on fluxes (aerosol radiative forcing), which is thought to offset partially the carbon dioxide greenhouse effect, presently remains one of the major sources of uncertainty in climate change studies (Charlson et al. 1992). The current paper seeks to document the physical basis and preliminary evaluation of aerosol retrievals over oceans made from the visible and infrared scanner (VIRS) aboard TRMM, in support of this aerosol radiative forcing objective. The major objective is to show how applying the operational Advanced Very High Resolution Radiometer (AVHRR) second-generation single-channel algorithm (Stowe et al. 1997) to two VIRS channels and deriving the Ångström exponent yield more information about aerosols that is useful for climate change studies with CERES data. In particular, the Ångström exponent provides an indication of whether particles are big or small, which is critical to understanding their radiative effects on climate (Lacis and Mishchenko 1995, and references therein).

VIRS is similar to the AVHRR aboard the National Oceanic and Atmospheric Administration's (NOAA) polar-orbiting satellites. Both have five channels, of which channels 1, 3, 4, and 5 are centered at $\sim$0.63, 3.7, 10.8, and 12 μm. Channel 2 is centered at $\sim$1.61 μm for VIRS and at $\sim$0.83 μm for AVHRR (Kidwell 1995; Barnes et al. 2000). Channels 1 and 2, measuring reflected solar radiation, are useful for aerosol retrievals. In section 2, we describe the algorithm for derivation of aerosol optical depths (AOD) in channels 1 and 2 τ_1^A and τ_2^A and the Ångström exponent α and discuss its

Corresponding author address: Dr. Alexander Ignatov, E/RA1, Rm. 712, WWBG, NOAA, 5200 Auth Rd., Camp Springs, MD 20746-4304.
E-mail: aignatov@nesdis.noaa.gov

premises, physical principles, and potential enhancements. We also compare our algorithm with alternate approaches proposed by other investigators for AVHRR. Greater spectral separation between channels on VIRS, as compared with AVHRR, should provide potentially more robust aerosol retrievals, assuming comparable measurement errors. We estimate theoretically the retrieval errors in section 3. Unfortunately, VIRS channel 2 is (unintentionally) strongly contaminated by a signal from another spectral interval, a thermal leak originating from a secondary spectral response peak at $\sim$5.2 μm. According to Dr. W. Barnes (1999, personal communication), a similar problem exists with moderate-resolution imaging spectroradiometer 1.6-μm data, thus making the methodology of the leak analysis presented here of potential interest and applicability for processing data from this sensor, as well. Details of the thermal leak correction can be found in section 4. In section 5, the derived parameters are evaluated empirically using a set of specially developed checks that reveal a high degree of self- and interconsistency of the retrievals. In sections 4–5, two types of VIRS data are used: pixel level, with original spacing of $\sim$(2 km)^2 at nadir and with a cloud mask appended; and single satellite footprint (SSF), representing spatial averages of VIRS pixel retrievals within a CERES footprint of $\sim$(25 km)^2. The third generation of SSF data (SSF-3) is used, in which dark count correction, derived in section 4, has already been incorporated into the processing stream. Note that this paper intends to demonstrate the principles and to outline generally the approach rather than to give a final account of the VIRS aerosol product and its accuracy. Work is under way to finalize the assessment of VIRS retrievals with the second-generation algorithm and to develop the next-generation aerosol product, which will provide substantial improvements over the current one. Major radiometric definitions used in the paper are summarized in the appendix.

2. Aerosol retrievals from reflectances in VIRS channels 1 and 2

a. Background

Radiation in a given spectral channel at a certain sun-view geometry, emerging from a cloud-free atmosphere bounded by a near-black ocean, is mainly moderated by the aerosol *scattering* AOD $\omega\tau^A$ [where τ^A is the *extinction*, or total, AOD, and ω is the single-scattering albedo (SSA)], and its phase function [$p^A(\chi)$]. These radiative properties, in turn, are complicated functionals of aerosol microphysics (i.e., particles' size distribution and shape, and complex index of refraction) and its vertical profile, particularly when observing in a region of the spectrum in which nonuniformly mixed gases absorb. This multifactor continuum of microphysical (or radiative) properties makes the problem of aerosol retrievals from a finite set of channels ill posed.

The number of independent measurements (channels) determines the maximum number of potentially derivable aerosol parameters. From the two VIRS measurements, no more than two independent aerosol parameters can be inferred; all other factors (both aerosol and nonaerosol, such as residual cloud, calibration errors, variations in the surface reflection) contribute to the retrieval errors. One needs to decide on the set of parameters and on the procedure to derive them. The parameters under retrieval, preferably, should be chosen to match those traditionally used in the community and measured from the ground to allow continuity and direct validation. In classic sun-photometry, spectral aerosol optical depth $\tau^A(\lambda)$ is measured (λ is wavelength), which is subsequently fit linearly in a log–log space as

$$\log\tau^A(\lambda) = \log\tau^A(\lambda_o) - \alpha \log(\lambda/\lambda_o) \qquad (1)$$

and is succinctly described by the two fit parameters—AOD at a reference wavelength $\tau^A(\lambda_o)$ and the Ångström exponent α (e.g., Smirnov et al. 1995). Derivation of this pair of parameters from AVHRR was proposed by Ignatov et al. (1998) and recently also was explored by Higurashi and Nakajima (1999) and Mishchenko et al. (1999).

To derive τ^A and α from satellite radiances with minimum error, one needs to construct a retrieval model and assume that all of its parameters other than τ^A and α are constant. The approach should be physically justified, consistent with the simplicity of the measurement scheme, and robust with respect to measurement errors and possible violations of the retrieval model. Clear structure, simplicity, and physical transparency of the algorithm allow for its efficient diagnosis and adjustments. To this end, the current VIRS retrieval algorithm is identical to the one that is used operationally with NOAA AVHRR data (Stowe et al. 1997). In channel 1, it derives τ_1^A using AVHRR's single-channel lookup table, LUT1. In channel 2, τ_2^A is retrieved using the same single-channel philosophy but with a different (yet aerosol-microphysically consistent) LUT2. Then, τ_1^A and τ_2^A are combined to estimate an effective Ångström parameter α. All retrievals are made in cloud-free conditions (P. Minnis et al. 1999, personal communication) on the antisolar side of the orbit ($\varphi > 90°$; φ is the relative azimuth), and outside of the sun-glint area ($\gamma > 40°$; γ is the glint angle defined so that $\gamma = 0$ when the satellite sensor is directed precisely toward the sun-glint area for a smooth ocean). The procedure itself, including its physical basis and premises, is documented and discussed in more detail below.

b. Retrieval algorithm

AOD in channel 1 τ_1^A is derived from VIRS channel 1 using a four-dimensional LUT1 ($14\theta_s \times 14\theta_v \times 19\varphi \times 7$AOD, where θ_s and θ_v are sun and view zeniths, and φ is relative azimuth) of overhead-sun albedos (see the appendix), precalculated using the Dave (1973) ra-

diative transfer (RT) model.[1] This VIRS LUT1 is similar to the one used in the AVHRR single-channel second-generation algorithm (Stowe et al. 1997), which is warranted by the radiometric near-identity of their channels centered at 0.63 μm. With one measurement, only τ_1^A is allowed to vary and all other oceanic and atmospheric parameters are prescribed. The algorithm's validity has been tested with AVHRR data from *NOAA-9* and *-11* against three ship sun-photometer datasets. Two of them (collected in 1989 and 1991) have been used to train the algorithm as mentioned above, and one (1988) is independent. All three consistently have shown an offset close to zero, a slope within $\pm 10\%$ of unity, and rmse$(\tau_1^A) \approx 0.04$. The algorithm and results of its validation with AVHRR historical data are described in greater detail in Ignatov et al. (1995a,b) and Stowe et al. (1997).

AOD in channel 2 τ_2^A is derived using LUT2, which is similar to LUT1, with a few distinctions: diffuse oceanic reflectance ρ_2^s is 0 instead of 2×10^{-3} used in LUT1 (ocean surface is assumed to be black); aerosol phase function is adjusted to channel-2 spectral interval (1.61 μm), with Mie calculations for the same microphysical aerosol model as in LUT1; Rayleigh optical depth τ_2^R is 0.0014 whereas τ_1^R is 0.060. Water vapor and carbon dioxide absorption correspond to the same midlatitude summer profiles, again adjusted to the spectral interval of channel 2.

An Ångström exponent α is then derived as

$$\alpha = -\ln(\tau_1^A/\tau_2^A)\ \ln(\lambda_1/\lambda_2), \tag{2}$$

when both τ_1^A and τ_2^A are greater than $\tau_{\min}^A$. A physically justified threshold $\tau_{\min}^A$, which must be used to cut off the inaccurate α retrievals at low aerosols (Ignatov et al. 1998), can be estimated from a combination of theoretical error analyses (cf. section 3), empirical consistency checks (cf. section 5), and future sun-photometer validation. In this study, it was preliminarily set to 3×10^{-2} to avoid indeterminancy and still allow analysis of the effect of $\tau_{\min}^A$ on α retrievals at small τ^A. This cutoff number should not be confused with a physically based threshold that is yet to be determined. Note that α is not a third, independent parameter, because it is derived from the two AODs. Rather, it can be considered as a different way of representing the retrieved aerosol information.

[1] Developed in the early 1970s, the Dave model has long been considered in the community as a standard for the multiple-scattering RT calculations in a multilayer atmosphere (e.g., Royer et al. 1988). However, it lacks some important features for real-world remote sensing applications, such as the Fresnel's reflection from a (rough) ocean surface, convolution of the upward spectral radiance with a finite spectral response of a channel, accurate atmospheric absorption, and flexibility of aerosol modeling. Evaluation of the Second Simulation of the Satellite Signal in the Solar Spectrum (6S; Vermote et al. 1997) is under way, to replace the Dave model. Some 6S calculations are used in this paper, for illustration purposes only.

c. Physics behind the retrievals

1) Simplified radiative transfer equation

A linearized single-scattering RT equation is used to illustrate physical principles of the algorithm and to guide its error analysis in section 3 (whereas actual retrievals are made using multiple-scattering Dave code–generated LUTs). According to Viollier et al. (1980) and Gordon and Morel (1983), the reflectance factor ρ (defined in the appendix) at the top of the ocean–atmosphere system is represented as

$$\rho_i = \rho_i^R + \rho_i^A + \rho_i^S T_i. \tag{3}$$

Here, i is the channel, ρ_i^R and ρ_i^A are Rayleigh and aerosol components, ρ_i^S (~ 0) is the ocean Lambertian component, and T_i is atmospheric transmittance[2] (which is typically of little importance for radiative transfer, because it is multiplied by a small oceanic reflectance term). The Rayleigh and aerosol components have a similar form:

$$\rho_i^R = P^R(\chi)\tau_i^R/(4\mu_s\mu_v),$$
$$\rho_i^A = [\omega_i P_i^A(\chi)]\tau_i^A/(4\mu_s\mu_v), \tag{4}$$

where $\mu_s = \cos\theta_s$; $\mu_v = \cos\theta_v$; $P^R(\chi)$ and τ_i^R are Rayleigh and $P_i^A(\chi)$ and τ_i^A are aerosol phase function and optical depths, respectively; ω_i is aerosol albedo of single scattering; and χ is scattering angle.

2) Physics of τ^A retrieval from a single channel

The Rayleigh and oceanic reflectances in Eq. (3) are well-constrained functions only of geometry, whereas the aerosol term is dependent on many more dramatically varying parameters. In single-channel retrievals of τ^A, the factor $[\omega P^A(\chi)]$, which is a functional of aerosol type, is prescribed and is kept nonvariable. For this procedure to work, the space–time variations of $[\omega P^A(\chi)]$ should be small when compared with the variations in τ^A. Over the oceans, τ^A varies within about two orders of magnitude, from $\sim 10^{-2}$ to ~ 1 in the visible (e.g., Smirnov et al. 1995). To assess variations of $[\omega P^A(\chi)]$ in backscatter ($\chi > 120°$), where aerosol retrievals are made, we use six standard aerosol models from the radiative transfer code 6S: Continental (CON), Maritime (MAR), Urban (URB), Desert (DES), Biomass Burning (BIO), and Stratospheric (STR; Vermote et al. 1997). These models are simpler than more sophisticated relative humidity–dependent models of Shettle and Fenn (1979) and d'Almeida et al. (1991). Yet, their full set presumably brackets the whole range of natural variability of aerosol types on the earth; in particular, over

[2] $T_i \approx \exp[-(1/\mu_s + 1/\mu_v)(0.5\tau_i^R + 0.13\tau_i^A)]$ (Viollier et al. 1980). Numerical estimates for $\mu_s = 0.5$–1.0, $\mu_v = 0.5$–1.0 give $T_1 \sim 0.53$–$0.94 \sim 0.75 \pm 0.20$ in channel 1 ($\tau_1^R = 0.06$, $\tau_1^A \sim 0$–1.0) and $T_2 \sim 0.60$–$1.00 \sim 0.80 \pm 0.20$ in channel 2 ($\tau_2^R = 0.0013$, $\tau_2^A \sim 0$–1.0).

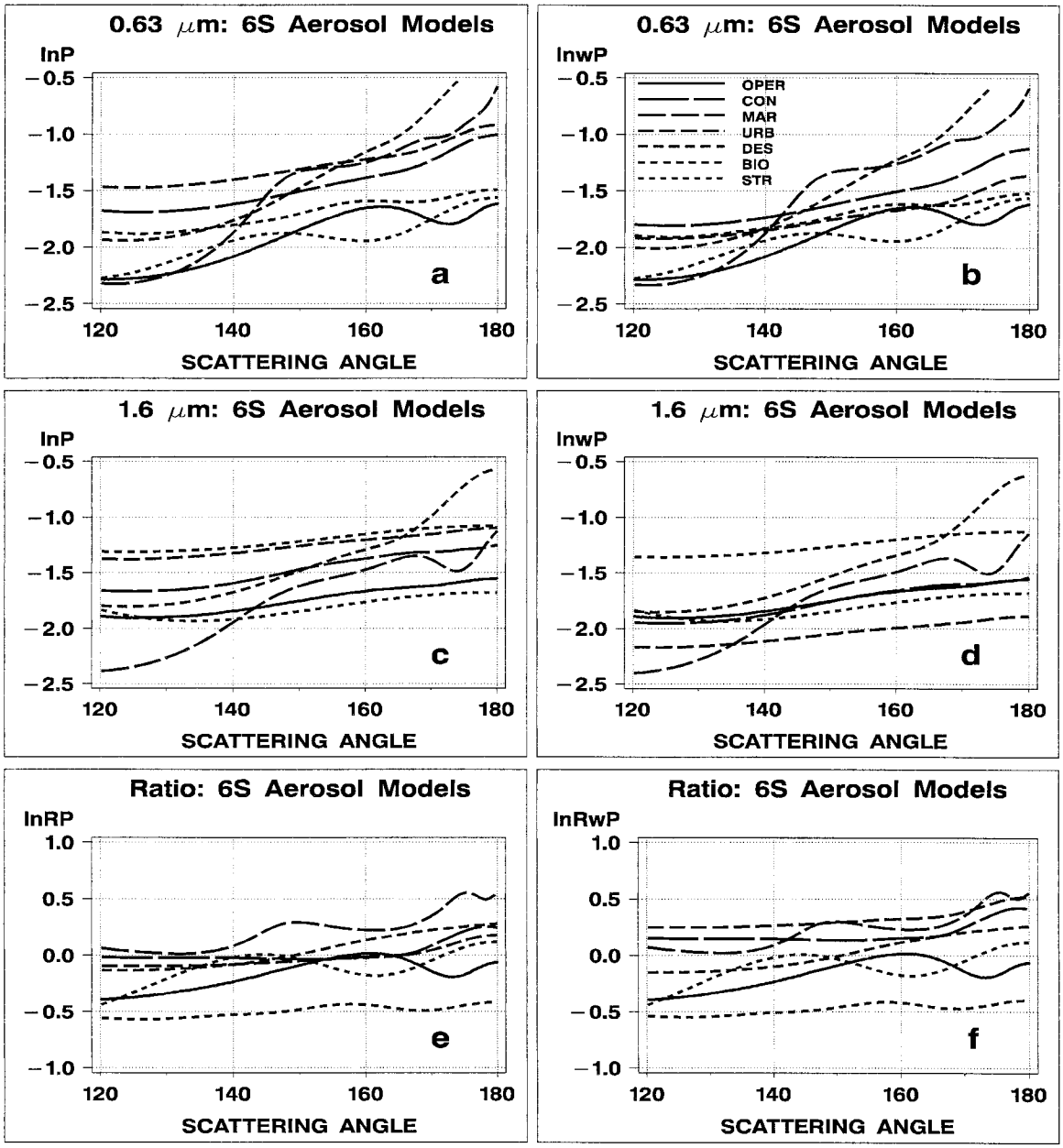

FIG. 1. The 6S model results for the six standard aerosol models (CON, MAR, URB, DES, BIO, and STR), and one microphysical model used in operational retrievals (monomodal lognormal size distribution $n(R) = dN/dR = [\sigma R(2\pi)^{1/2}]^{-1} \exp[-\ln(R/R_m)^2/2\sigma^2]$, with $R_m = 0.1$ μm, $\sigma = \ln(2.03)$, and $n = 1.40 - 0.0i$ (OPER) in VIRS channels 1 and 2 (0.63 and 1.61 μm, respectively). The x axis is always scattering angle χ. The y axis shows, on linear scale: (a) ln$P$: natural logarithm of the model phase functions in channel 1, $\ln[P_1^A(\chi)]$; (b) lnwP: natural logarithm of single-scattering albedo–adjusted phase functions in channel 1, $\ln[\omega_1 P_1^A(\chi)]$; (c) same as (a) but in channel 2: $\ln P = \ln[P_2^A(\chi)]$; (d) same as (b) but in channel 2: $\ln wP = \ln[\omega_2 P_2^A(\chi)]$; (e) natural logarithms of ratios of phase functions: $\ln RP = \ln[P_1^A(\chi)/P_2^A(\chi)]$; (f) natural logarithms of ratios of the SSA-corrected phase functions: $\ln R\omega P = \ln\{[\omega_1 P_1^A(\chi)]/[\omega_2 P_2^A(\chi)]\}$. Note: The use of natural logarithm in (a)–(d) allows easy estimate of percent difference in phase functions. For instance, a 0.1 in $\ln(X)$ [where $X = (P^A)$ or $X = (\omega P^A)$] corresponds to an ~10% difference in X and, subsequently, to a 10% error in τ^A. In (e)–(f), the use of natural logarithm allows easy estimate of equivalent error in α: $\delta\alpha \sim \Lambda\delta \ln R\omega P \approx \delta \ln R\omega P$, because $\Lambda = 1.1 \approx 1$ (see also section 3b).

the oceans, where different aerosols may be encountered. (In fact, any significant elevation of AOD above its marine background level of $\tau^A \approx 0.1$ may be indicative of particle intrusion from either a continent—CON, DES, URB, BIO—or from a volcanic eruption—STR).

Figures 1a–d show $\ln[P^A(\chi)]$ and $\ln[\omega P^A(\chi)]$ versus scattering angle in the two VIRS channels, and Fig. 2c

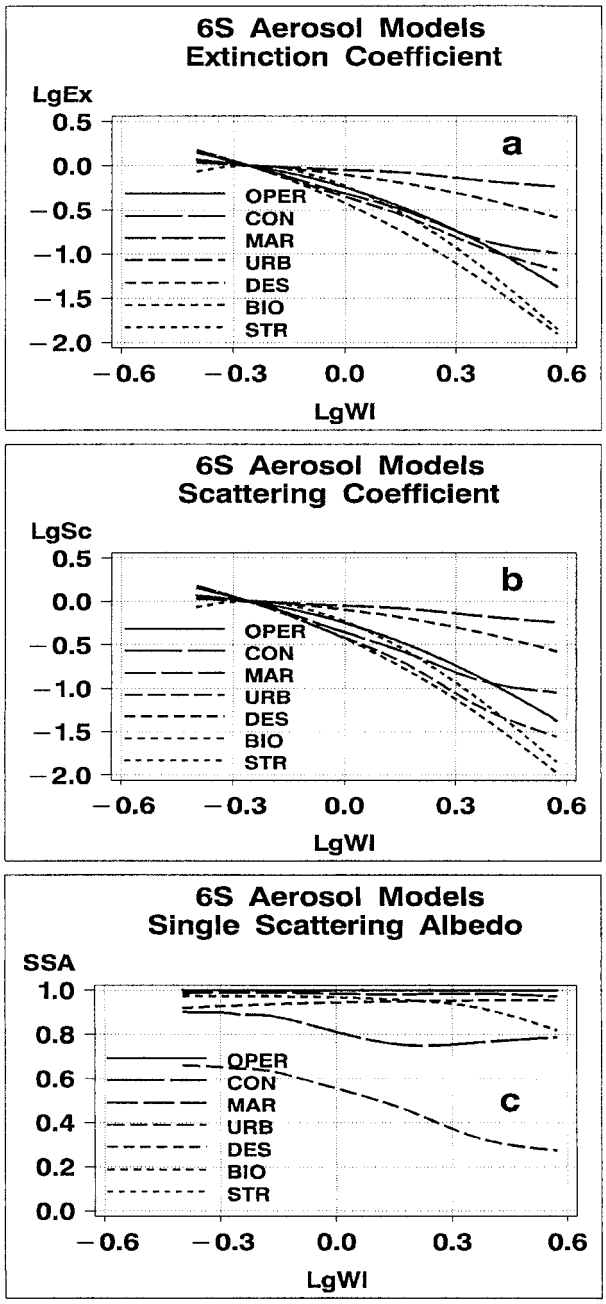

FIG. 2. Decimal logarithms of (a) extinction and (b) scattering coefficients (both normalized at 0.5 μm), and (c) SSA versus decimal logarithm of wavelength. See caption to Fig. 1 for model details.

gives spectral SSAs for these models. Typically, ωs in the two VIRS channels are within a few percent of unity (except for CON and URB, for which ω deviates from unity significantly), and close to one another. Figure 1 suggests that the intermodel variability in $[\omega P^A(\chi)]$ is within $\approx\pm 10\%$–50%, depending upon scattering angle (hereinafter, we use $\pm 30\%$ to represent average scattering geometry). This variability is not negligible, but yet, it is much less than the variability in τ^A itself (cf. Quenzel and Kaestner 1980; Kaufman 1993), thus providing the premise for using a prescribed aerosol model for the single-channel retrieval algorithm of τ^A. This estimate of error recently has been independently confirmed by rigorous AVHRR retrievals with a representative set of aerosol microphysical models (Mishchenko et al. 1999), for which the sensitivity of τ^A to aerosol model was found to be well within $\sim\pm 30\%$ (cf. their Figs. 18b–d). Note that larger errors of τ^A observed in their Fig. 18a (up to 300%, as the authors claim) are due to the unrealistically big particles assumed in this particular global retrieval, which are only likely to occur downwind of deserts (d'Almeida et al. 1991).

For unbiased retrievals, the phase function used in NOAA operations (see Stowe et al. 1997 and the caption to Fig. 1) $[P^A(\chi)]_{\text{oper}}$ should fall somewhere in between the model calculations. As shown in Fig. 1, for channel 2, $[P_2^A(\chi)]_{\text{oper}}$ (solid line; $\omega \equiv 1$) falls well in between the $[\omega_2 P_2^A(\chi)]$ for the standard 6S models. In channel 1, however, Fig. 1b shows that $[P_1^A(\chi)]_{\text{oper}}$ is closer to the lower boundary of the family of model curves.

3) ÅNGSTRÖM EXPONENT RETRIEVAL

The Ångström parameter α varies between 0 and 2 in natural conditions (e.g., Smirnov et al. 1995). For the aerosol model used in the VIRS retrievals, $\alpha_o = -\ln(\beta_1^{\text{ext}}/\beta_2^{\text{ext}})/\ln(\lambda_1/\lambda_2) \sim 1.25$, where β_i^{ext} is the extinction coefficient in channel i. It may seem that using this model to retrieve τ_1^A and τ_2^A invariably results in $\alpha \equiv \alpha_o$, no matter what the real Ångström exponent is. In fact, the retrieved α tends to be closer to the real α than to α_o, as explained in the next paragraph.

Analysis of the previous section shows that the retrieved τ_1^A and τ_2^A are subject to multiplicative errors when actual $[\omega_1 P_1^A(\chi)]$ and $[\omega_2 P_2^A(\chi)]$ deviate by up to $\sim\pm 30\%$ from those assumed in retrievals [Eq. (4)]. However, multiplicative errors in τ_1^A and τ_2^A will cancel out while taking the ratio in Eq. (2) if they are about the same in the two channels. Some studies show that P^A, although it changes depending upon the microphysics and chemistry of the particles, is still close to being spectrally neutral in the visible and near-infrared (e.g., Viollier et al. 1980; Gordon and Morel 1983). As a result, even though the real $[\omega_1 P_1^A(\chi)]$ and $[\omega_2 P_2^A(\chi)]$ depart from those assumed in the retrieval model and show large variability with scattering angle, their ratio is close to unity and is substantially less variable with scattering angle (cf. Figs. 1b,d,f and the discussion in section 3). As a result, the estimated Ångström exponent is less subject to error from an incorrect aerosol model than are the τ^As from which it is derived. This result, which has been arrived at here using simple physical considerations, has been confirmed recently by rigorous numerical retrievals from AVHRR by Mishchenko et al. (1999), who suggest that the Ångström exponent "is the aerosol size characteristic least sensitive to the un-

certainties in the atmosphere–ocean model and should be retrieved along with optical thickness as the second aerosol parameter.''

d. Premises and potential enhancements to the retrieval algorithm

1) PREMISES OF THE CURRENT APPROACH

The current two-independent-channel algorithm is simpler than the more traditional simultaneous solution procedure, which uses multidimensional LUTs created from variable aerosol models to estimate the two aerosol parameters at once from the two radiances. The former may be less accurate for α and even less accurate for τ^A retrievals, but it is more robust and better structured. Its lends itself to highlighting and checking different logical steps used in the retrieval that are separated from each other. Independent AOD retrievals allow easier identification and removal of errors in either channel, which is particularly important if some of them are known to have problems, such as the thermal leak in channel 2. The two independent retrievals in channels 1 and 2 are quality controlled and consistency checked, individually, before combining them further to estimate α, which, in turn, is tested and checked.

Thus, the independent-channel approach has been adopted, initially, for VIRS, because of our operational experience with it from NOAA AVHRR analyses, and because it could easily be implemented into the VIRS processing stream. This simple procedure works reasonably well, as shown later, but also may be easily improved upon. For example, after τ_1^A and τ_2^A have been retrieved and α derived therefrom, the retrieval aerosol model (phase function) may be adjusted to match better the derived α, and the retrieval procedure may be iterated until it converges. In addition, the first iteration potentially may be improved if parameterization of the factor $[\omega P^A(\chi)]$ as a function of τ^A proves possible, which may reduce the number of iterations (Kaufman 1993). These considerations serve as a basis of the next-generation retrieval algorithm presently under development.

2) STRUCTURED VERSUS UNSTRUCTURED APPROACHES

Examples of alternate approaches for the AVHRR that potentially can be generalized to be used with VIRS are given by Durkee et al. (1991, 2000), Nakajima and Higurashi (1997), Higurashi and Nakajima (1999), Geogdzhayev and Mishchenko (1999), and Mishchenko et al. (1999). Only Durkee et al. (1991, 2000) offer a structured approach by which the ratio of Rayleigh-adjusted reflectances in channels 1 and 2 is first related theoretically to different phase functions, then is used to predict phase functions in both channels, which, in turn, are used to retrieve τ^As. In the four other algorithms, the two-channel reflectances are fed as simultaneous input into a multidimensional LUT with variable aerosol models, and τ^A and ν (Junge size parameter; Nakajima and Higurshi 1997; Geogdzhayev and Mishchenko 1999) or τ^A and α (Higurashi and Nakajima 1999; Mishchenko et al. 1999) are estimated at once. On the positive side, they do not require iterating or multiple paths through the data; on the negative side, the analyses of the individual contributions from the channels are problematic, and departures from the assumed type of aerosol size distribution in the LUTs may be a large source of error. For operational applications, these more complex yet computationally efficient procedures should be implemented after all possible diagnostic issues are understood and resolved with independent channel approaches.

3) ÅNGSTRÖM VERSUS NON-ÅNGSTRÖM FORMULATIONS

Equation (2) is the definition of an ''effective'' Ångström exponent for the pair of wavelengths λ_1–λ_2. Figure 2 suggests that, in general, the Ångström law may be violated over a wide spectral range, and a quadratic (rather than linear) log–log fit seems more appropriate (King et al. 1980). Still, the effective Ångström exponent defined by Eq. (2) is a useful parameter indicative of particle size. However, caution must be used when applying it to reconstruct extinction within the spectral interval λ_1–λ_2 or extrapolating it into other spectral intervals.

Derivation of other aerosol size parameters, such as the Junge exponent ν (e.g., Nakajima and Higurashi 1997; Geogdzhayev and Mishchenko 1999), an effective particle radius (Mishchenko et al. 1999), or a ''mixing ratio'' η of the two modes in a bimodal lognormal distribution (Tanre et al. 1997) can be attempted, based on the assumed type of aerosol size distribution. In many of the ''non-Ångström'' formulations, however, α can still be estimated by substituting the retrieved τ^As (estimated from a set of retrieved aerosol parameters, whatever they may be, but consistent with the retrieval model) into Eq. (2). Vice versa, the parameters used in different formulations can be estimated from a known Ångström exponent, provided some assumptions consistent with the aerosol microphysical model are made. We suggest that all retrieval methods should provide an Ångström exponent parameter to be used as a standard for intercomparison of the various formulations.

Use of the Ångström exponent seems advantageous to us for a number of reasons. First, in comparison with other models, its derivation requires the least amount of restrictive a priori assumptions, which is good, considering the fact that ''it is not easy to distinguish between different aerosol size distributions from remote sensing observations'' (Kaufman et al. 1997). Also, this parameter has been widely used in the community for many years. As a result, the researchers are accustomed

to it, and significant experience and intuitive knowledge has been gained on its expected ranges of variability, accuracy, and relation to different air masses. It is routinely derived from customary sun-photometers, allowing direct validation of the satellite retrievals.

3. Theoretical error analysis of VIRS retrievals

Error analysis in this section, based on the analytical RT Eqs. (3)–(4) as proposed by Ignatov et al. (1998), seeks to demonstrate major error sources and trends in τ^As and αs from VIRS. Use of a more comprehensive and accurate analytical formulation of the RT equation is possible (e.g., Wagener et al. 1997) but would complicate the sensitivity formulas and therefore is not attempted here.

We stress that all numerical estimates in sections 3a,b are worst-case-scenario errors for individual measurements, in which the magnitudes of all errors are added without consideration of sign. Typical statistics of errors (e.g., root-mean-square errors) would be much lower, especially if some averaging in space and time is applied to the data. These more realistic errors are discussed in section 3c.

a. Errors in τ^A

From Eqs. (3) and (4), τ^A is derived as

$$\tau^A = \frac{4\mu_s\mu_v}{[\omega P^A(\chi)]}(\rho - \rho^R - \rho^S T). \tag{5}$$

Differentiating Eq. (5), one obtains an expression for the error δ in τ^A:

$$\delta\tau^A = \frac{\delta[\omega P^A(\chi)]}{[\omega P^A(\chi)]}\tau^A + \frac{4\mu_s\mu_v}{[\omega P^A(\chi)]}(C - \mathrm{DC})\delta S + \frac{4\mu_v}{[\omega P^A(\chi)]}\delta\mathrm{DA} + \frac{P^R(\chi)}{[\omega P^A(\chi)]}\delta\tau^R + \frac{4\mu_s\mu_v T_o}{[\omega P^A(\chi)]}\delta(\rho^S). \tag{6}$$

Here, the differential $\delta\rho$ of the measured signal is replaced by $\delta\rho = [(C - \mathrm{DC})\delta S - S\delta\mathrm{DC}] \equiv [(C - \mathrm{DC})\delta S - \delta\mathrm{DA}/\mu_s]$, where DA is the dark albedo defined in the appendix as $\mathrm{DA} = \mu_s S\mathrm{DC}$.[3] Equation (6) shows that errors in τ^A are due to errors from five sources (terms on the right-hand side): aerosol model, measured radiance (slope and dark count), Rayleigh optical depth, and surface diffuse reflectance, respectively. For simplicity, the following error analyses of the above five factors are done separately, assuming the other four are fixed when analyzing the errors resulting from the one selected for analysis (partial derivative approach).

1) MULTIPLICATIVE AND ADDITIVE ERRORS IN τ^A

There are two types of error in τ^A: those proportional to τ^A (referred to as *multiplicative errors*) and those independent of τ^A (referred to as *additive errors*). The first term on the right-hand side of Eq. (6) is the error from the deviation of the actual aerosol model from that assumed in the retrieval. This component of error is largely coherent in both channels, $\delta\tau^A \sim \tau^A(\delta\omega P^A/\omega P^A)$, where $\delta\omega P^A/\omega P^A$ may reach up to $\pm 30\%$ for an average scattering geometry, as Figs. 1b,d suggest. This error in optical depth becomes dominant at high τ^A (when $\rho^A \gg \rho^R + \rho^S T$, i.e., $\rho \sim \rho^A$), but progressively decreases at low τ^As. The second component in Eq. (6) is either multiplicative or additive, in the two extreme situations of low and high aerosol amounts, respectively. At high aerosols, it is approximated as $\delta\tau^A \sim \tau^A(\delta S/S)$. The latter estimate comes from noting in Eq. (5) that $\delta\tau^A/\tau^A = \delta\rho/\rho$, and substituting the calibration formula for ρ in Footnote 3, making the total multiplicative error $\delta\tau^A \sim \tau^A(\delta\omega P^A/\omega P^A + \delta S/S) \sim \pm 0.35\tau^A$. (Typically, $\delta S/S \sim 0.05 \ll \delta\omega P^A/\omega P^A$.)

The error resulting from slope uncertainty at low aerosols, and the three remaining components of error in Eq. (6) (from uncertainties in dark count, Rayleigh, and ocean reflectance) are additive. As a result, their relative contribution decreases at high aerosols but becomes progressively more important at low aerosols and fully determines the error budget at the low end of the retrieved τ^A (when $\tau^A \to 0$, i.e., $\rho \sim \rho^R + \rho^S T_o \gg \rho^A$). Below, numerical estimates of the *additive error* pertinent to VIRS channels 1 and 2 are discussed, assuming μ_v, $\mu_s \sim 0.5$–1.0, and $(\omega P^A) \sim 0.2$ (cf. Figs. 1a–d).

2) ERRORS IN CHANNEL 1

The largest error in τ_1^A may come from the combined effect of calibration and Rayleigh optical depth, which are almost indistinguishable at low τ^As. Indeed, when $\tau^A \to 0$, the measured signal is mainly due to Rayleigh scattering ($\rho^R \gg \rho^A + \rho^S T$, i.e. $\rho \sim \rho^R$), so that error in τ^A is $\delta\tau_1^A \sim \tau_1^R(P^R/\omega P^A)(\delta\tau_1^R/\tau_1^R + \delta S_1/S_1)$. A 10% combined calibration/Rayleigh error ($\delta\tau_1^R/\tau_1^R + \delta S_1/S_1 \sim 0.1$) would lead to an error of $\delta\tau_1^A \sim \pm(3$–$5) \times 10^{-2}$ (hereinafter, the en-dash brackets the range of possible variations in a parameter, in particular, because of variable sun-view geometry, etc.). The oceanic Lambertian reflectance term is composed of an underwater signal and foam reflectance. Over open oceans, the total reflectance in channel 1 is $\rho_1^S \sim 2 \times 10^{-3}$ (e.g., Ignatov et al. 1995a). Assuming that its variability is on the order of magnitude of ρ_1^S itself [$\delta\rho_1^S \sim (2 \pm 2) \times 10^{-3}$], Eq. (6) gives $\delta\tau_1^A \sim \pm(1$–$3) \times 10^{-2}$ [cf. with Frouin et

[3] Note calibration formula: $\rho = S(C - \mathrm{DC})$, where S is calibration slope, C is Earth-viewing signal count (assumed not to be subject to error), and DC is dark count, which is signal viewing a black target and is usually a constant. However, for VIRS channel 2, it is a function of the Earth-viewing temperature, because of an infrared leak in its filter as discussed in section 4.

al. (1996) who give an estimate of $\delta\tau_1^A \sim \pm 2 \times 10^{-2}$, from only the foam part of the Lambertian reflectance]. Over turbid waters (e.g., in coastal areas), the surface underwater reflectance may reach $\rho_1^S \sim 5 \times 10^{-3}$ or more, leading to an additive error $\delta\tau_1^A$ of up to $+(3\text{–}10) \times 10^{-2}$ (note that this type of error always results in an overestimate in τ^A, because elevation of the satellite signal caused by the brighter surface is interpreted by the algorithm as an increase in aerosol content).

In summary, the combined multiplicative and additive "worst-case" error for channel 1 is $\text{Max}(\delta\tau_1^A) \sim \pm 0.35\tau_1^A \pm (0.04\text{–}0.08)$ over open oceans, and may reach $\text{Max}(\delta\tau_1^A) \sim \pm 0.35\tau^A \pm (0.04\text{–}0.08) + (0.03\text{–}0.10)$ over coastal waters.

3) Errors in channel 2

The Rayleigh/calibration-related additive error would be ~40 times less in this channel, in proportion to the value of $\tau_2^R \sim (1/40)(\tau_1^R)$, that is, on the order of $\delta\tau_2^A \sim 1 \times 10^{-3}$. A critical additive error in this channel results from a residual thermal leak signal: $\delta\tau_2^A \sim 4\mu_v \delta\text{DA}_2/[\omega_2 P_2^A(\chi)]$. Substituting $\text{Max}(\delta\text{DA}_2) \sim 1.5 \times 10^{-3}$ in the above formula (see section 4), one obtains a maximum error of $\text{Max}(\delta\tau_2^A) \sim (1.5\text{–}3.0) \times 10^{-2}$. The oceanic reflectance term is negligible over open oceans (away from the specular reflection), so that it supposedly does not contribute to error in τ_2^A. According to Frouin et al. (1996), foam gives $\delta\tau_2^A \sim \pm 1 \times 10^{-2}$. Over turbid waters, we assume the same underwater signal as in channel 1: $\rho_2^S \sim 5 \times 10^{-3}$, which leads to an additive error $\delta\tau_2^A$ up to $+(3\text{–}10) \times 10^{-2}$.

In summary, the worst-case error is $\text{Max}(\delta\tau_2^A) \sim \pm 0.35\tau_2^A \pm (0.03\text{–}0.04)$ over open oceans, and may reach $\text{Max}(\delta\tau_2^A) \sim \pm 0.35\tau_2^A \pm (0.03\text{–}0.04) + (0.03\text{–}0.10)$ over coastal waters.

b. Errors in α

The Ångström parameter varies in natural conditions between ~0 and 2 (e.g., Smirnov et al. 1995), which gives a reference against which the potential errors in the derived α are to be measured. According to Eq. (2), the error in α is amplified by a spectral separation factor, $\Lambda = -1/\ln(\lambda_1/\lambda_2)$. For VIRS, $\Lambda \sim 1.1$, versus $\Lambda \sim 3.6$ for AVHRR, suggesting that retrievals of α from VIRS should be more robust than from AVHRR, assuming comparable errors in the retrieved τ^A values (but perhaps may need a different interpretation, because of sensitivity to larger particles).

1) Errors in α from multiplicative errors in τ^A

Definition of α through a ratio of τ^As leads to different effects of multiplicative and additive errors in τ^A on α. For the aerosol model–related component (i.e., ignoring errors in aerosol path reflectance) of error, Eq. (2) gives $\delta\alpha = \Lambda\delta\ln(\tau_1^A/\tau_2^A) \sim \Lambda\delta\ln\{[\omega_1 P_1^A(\chi)]/[\omega_2 P_2^A(\chi)]\}$. Figure 1f, which shows $\ln\{[\omega_1 P_1^A(\chi)]/[\omega_2 P_2^A(\chi)]\}$ for the six standard 6S models, suggests that the resulting error in α depends upon the type of aerosol and scattering geometry, and may reach, in the worst case, $\text{Max}(\delta\alpha) \sim \pm 0.5$. At large AOD, another multiplicative error, resulting from calibration errors, is much smaller (e.g., even 5% calibration errors of opposite sign in the two channels only raise this estimate by $\sim \pm 0.1$).

2) Errors in α from additive errors in τ^A

Because additive errors in τ^A do not depend upon τ^A itself, their effect on α increases at low AOD, thus resulting in an error in α that is inversely proportional to τ^A (Ignatov et al. 1998). This effect can be somewhat controlled by making retrievals at $\tau^A > \tau_{\text{min}}^A$ only, where τ_{min}^A should be chosen consistently with τ^A errors in both channels. The definition of τ_{min}^A may involve issues such as whether the data are averaged in space and/or time, and, if so, is this averaging performed with weights proportional to τ^A, as proposed by Mishchenko et al. (1999). Some errors may be considered random or systematic, depending upon the space–time ensembles. One should, however, always expect errors in α, if observed, to be inversely proportional to τ^A. If no averaging is applied, then the previous analysis suggests that, to achieve $\text{Max}(\delta\alpha) \sim \pm 0.5$ for individual measurements, the additive errors in individual τ^As must not exceed 25%. From the analyses in section 3a, such accuracy is possible when $\tau_1^A > 0.15\text{–}0.30$, and $\tau_2^A > 0.10\text{–}0.15$ over open oceans. Over coastal turbid waters, the thresholds are respectively higher.

c. Reduction of errors in τ^A and α

Multiplicative errors, important at large AODs, are mainly due to the assumption involved in the aerosol retrieval model. These errors are probably better treated with *simultaneous* retrievals of τ_1^A, τ_2^A, and α, but they cannot be alleviated completely, because one cannot fully avoid the need for making aerosol model–related assumptions. A *simultaneous* approach can be considered once nonaerosol-related errors (such as, e.g., errors from uncertainties in calibration, ocean reflectance, or Rayleigh) are minimized, which is best done by keeping the retrievals in two channels independent.

Additive errors can be reduced by a more careful choice of spectral responses of the channels to avoid contamination from other spectral intervals, such as the thermal leak in VIRS channel 2, and more precise calibration of the radiometer. [Note that VIRS radiometric calibration, analyzed in detail by Lyu et al. (2000), has not shown noticeable errors so far, but errors as large as 15% in channel 2 have been inferred through derived parameter validation studies and intercomparisons with other sensors (P. Minnis 1999, personal communication).]

Random errors, both multiplicative and additive, can be reduced by averaging data in space (as is done, for example, in the CERES SSF product) or in time. Up to 100 VIRS measurements are found within an SSF ''pseudopixel,'' which would reduce all random errors ~10 times, if independent. However, they are not fully independent, thus reducing this coefficient, and one can tell only empirically to what extent. Some errors are always systematic (such as errors that are due to calibration uncertainty), and some may be considered as systematic or random depending upon the ensemble (space–time-averaging domain; e.g., Rayleigh optical depth/aerosol phase function/ocean reflectance/thermal leak, etc.). The question of reduction of the random error always needs individual analysis.

d. Discussion of errors in τ^A and α

The above error analysis principles can be applied to both satellite and sun-photometer retrievals of τ^A. For identical spectral channels, errors are obviously larger for the satellite, because of more interfering factors being involved (and therefore more assumptions are needed to remove them from the product). The derivation of α, which depends on AOD from only two spectral measurements, was known to be problematic even for sun-photometers, as discussed at the time such measurements were proposed (Ångström 1961, 1964). In close analogy with τ^A, the derivation of α from two-channel satellite measurements is therefore likely to be even less accurate than from sun-photometer. This fact suggests that two measurements may be insufficient for reliable estimation of two aerosol parameters. This is because of many different uncertainties/errors in the measurements and required assumptions that make the problem of solving two equations with two unknowns ill posed. This problem is fundamental to aerosol remote sensing, and it cannot be removed by using another size parameter as an alternative to α, such as, for example, Junge parameter, or an effective particle radius. What is more, the use of any parameter other than α does not even seem to alleviate its severeness mathematically. The analyses of Mishchenko et al. (1999) suggest, for instance, that the Ångström exponent turned out to be the most robust aerosol size parameter, out of three they have considered (the physical reasons being, largely, cancellation of the phase functions while taking the ratio of aerosol optical depths, or path radiances). The mainstream approach to improving the accuracy of aerosol size parameter (be it α or another one) from spectral measurements is widening the spectral range spanned by the sun-photometer or satellite channels and raising the number of channels. This approach would allow improvements in the accuracy because of the fact that, mathematically, the problem is better posed.

4. Dark albedo analyses

Processing the original VIRS radiances into optical depths results in τ_2^A values, which exceed τ_1^A by amounts comparable to τ_1^A itself (see Fig. 5a). This is caused by a leak of thermal radiation through a secondary transmittance peak in the channel-2 filter at 5.2 μm [see Fig. 6 of Barnes et al. (2000)]. The thermal signal from this leak must be removed from the daytime observations before accurate aerosol retrievals can be made with this channel. As can be seen in Fig. 5b, the correction reduces the additive error caused by the leak to a level that makes retrievals of τ_2^A and α reasonable, particularly at higher optical depths, where estimates of particle size are most important. The knowledge of size parameter for climate modelers is of little importance at low τ^A and gradually increases with τ^A—that is, exactly when better accuracy can be achieved.

Theoretical correction, based on convolution of modeled upward thermal radiance of the ocean–atmosphere system with the channel's spectral response, was considered but rejected, because of its many potential uncertainties, in favor of an empirical approach. A special after-launch effort was undertaken, in cooperation with the National Aeronautics and Space Administration (NASA) Goddard Space Flight Center (GSFC) group headed by Dr. C. Kummerow, to collect nighttime VIRS data in a daytime mode. (Nighttime data are defined as those with $\theta_s > 95°$, i.e., 5° beyond the terminator; data within 5° of the terminator still show a sizeable solar reflected component.) This collection was first done on an initial test day of 20 February 1998, and, as of 8 April 1998, all channel data have been archived continuously, both day and night. The nighttime data are analyzed to quantify the effect of a thermal leak in channel 2 as a function of radiances in channels 4 and 5 (R_4 and R_5) and view angle θ_v. Channel-2 daytime measurements are subsequently corrected for the effect of the thermal leak by subtracting the emission component of the signal estimated by applying these nighttime parameterizations to daytime measurements.

The leak has its maximum effect on cloud-free observations (those used for aerosol retrievals), for two reasons: 1) the underlying ocean is the warmest scene, and 2) the reflected component of radiation is at its lowest, resulting in the maximum emitted (thermal) signal being added to the minimum reflected signal. Over colder cloud, the thermal component decreases and the reflectance increases, making the effect progressively less important for tasks related to cloud detection and retrieval, pursued by other investigators on the TRMM Science Team. The CERES team, however, requested that a general thermal-leak correction algorithm be developed, applicable for correction of all-sky reflectances and not just the clear-sky subset. The applicability of the all-sky derived correction to the clear-sky subset and to aerosol retrievals from it was confirmed by showing

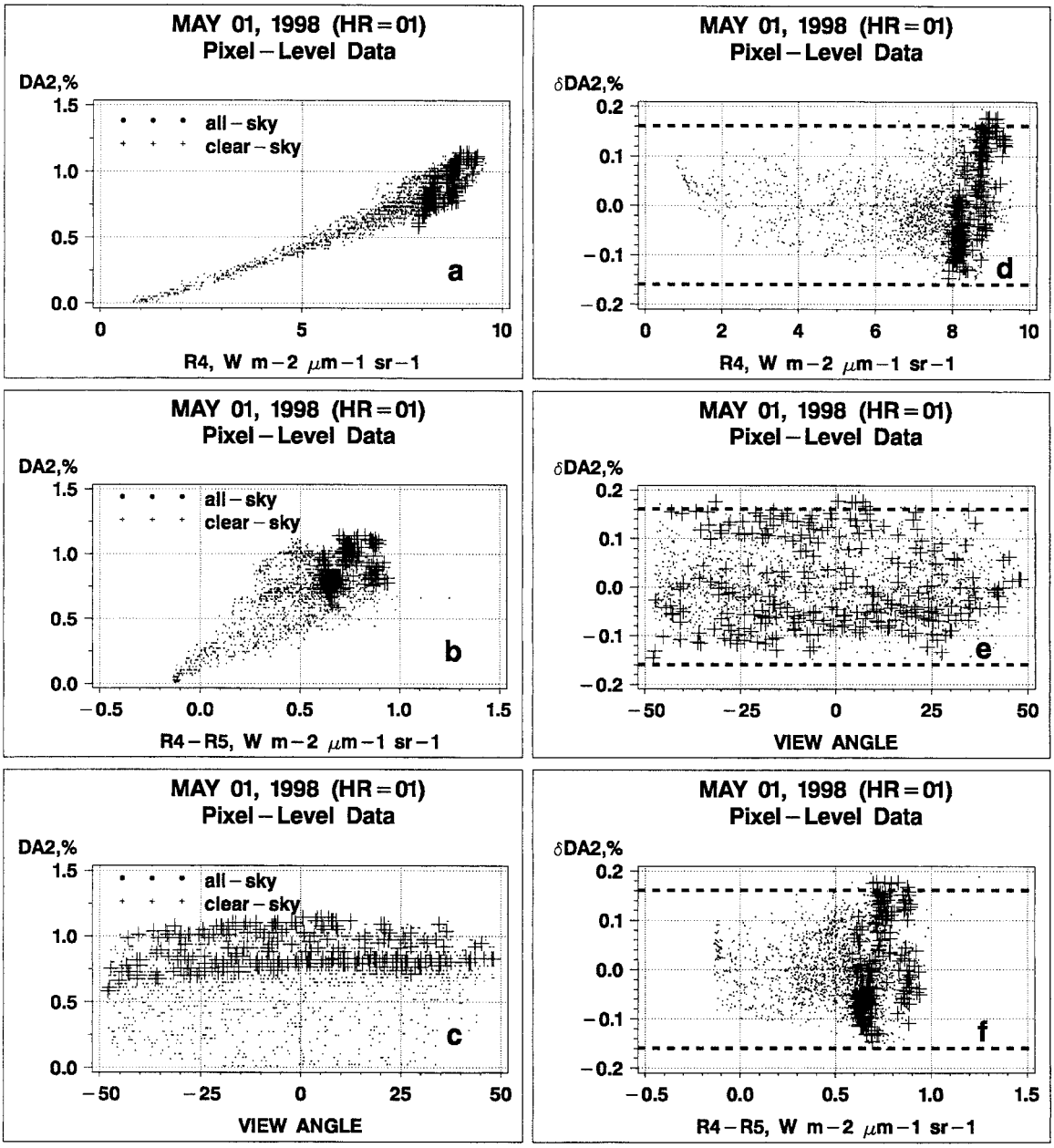

FIG. 3. (a)–(c) Dark Albedos in channel 2 versus radiance in channel 4 ($R4$), channel 4–5 difference ($R4 - R5$), and view angle (θ_v). (d)–(f) Residual error after multiple regression prediction equation of Table 1 was applied. [HR is hour (UTC) of satellite observations, and horizontal dashed lines indicate the extremes in variability.]

that the resulting bias error in τ^A was $\sim\pm 0.01$. It was decided to tolerate this residual error, for the sake of the integrity of the VIRS processing stream.

a. Derivation of ''dark albedo'' from nighttime data

Nighttime VIRS ''dark'' albedos (see appendix for definition) were analyzed for 1 May 1998. For channel 1, the maximum dark albedo error $\mathrm{Max}(\mathrm{DA}_1)$ was found to be less than 10^{-4} (not shown), whereas for channel 2, $\mathrm{Max}(\mathrm{DA}_2) \sim 1.2 \times 10^{-2}$ (see Fig. 3, left). According to Eq. (6), this value is equivalent to maximum errors $\mathrm{Max}(\delta\tau_1^A) \sim (0.7\text{–}1.4) \times 10^{-2}$ and $\mathrm{Max}(\delta\tau_2^A) \sim 0.12$–0.25. Thus, it was decided that the error in channel 1 could be neglected, but in channel 2, where it is comparable to or exceeds the expected τ_2^A over oceans, it needed to be corrected.

As Fig. 3a shows, the dependence of DA_2 on radiance

TABLE 1. Regression coefficients for dark-albedo analysis $DA_2 = A_0 + A_R R_4 + A_{DR}(R_4 - R_5) + A_{\theta 1}\theta_v + A_{\theta 2}\theta_v^2$ on 1 May 1998 (all coefficients are $\times$ 1000).

A_0	A_R	A_{DR}	$A_{\theta 1}$	$A_{\theta 2}$
-226.3 ± 0.7	157.1 ± 0.2	-304.9 ± 1.3	0.453 ± 0.006	-0.0240 ± 0.0003

in channel 4 (R_4) is close to linear.[4] Under cloud-free conditions (highest values of R_4), the correlation becomes weak, because the two spectral intervals (5.2 and 10.8 μm) are sensitive, not only to the total amount of water vapor, but to its vertical stratification in the atmosphere. Figure 3b confirms that the difference between radiances in channels 4 and 5, $R_4 - R_5$, can be used as a measure of this secondary effect (e.g., McClain et al. 1985). Figure 3c suggests that there is also a (weak) quadratic trend against view angle that may be considered to be a third-order effect. In summary, DA_2 is parameterized as

$$DA_2 = A_0 + A_R R_4 + A_{DR}(R_4 - R_5) + A_{\theta 1}\theta_v + A_{\theta 2}\theta_v^2. \quad (7)$$

Multiple regression analyses have been performed over the all-sky pixel-level data. The derived coefficients are listed in Table 1, and Figs. 3d–f show residuals of the correction δDA_2. The $\mathrm{Max}(\delta DA_2) \sim 1.5 \times 10^{-3}$, which is equivalent, according to Eq. (6), to $\mathrm{Max}(\delta\tau_2^A) \sim (1.5$–$3.0) \times 10^{-2}$. Figure 4 shows the frequency distributions of the original DA_2 and its residual δDA_2. (The secondary peak in the two histograms might indicate a third minor spectral response in VIRS channel 2, in addition to the 5.2-μm secondary peak, or may result from nonuniform sampling of the surface.)

b. *Application of dark albedo correction to daytime data*

In daytime, VIRS channel-2 albedo A_2 is corrected for the thermal leak by subtracting DA_2 from it, that is, $(A_2 - DA_2)$. Albedo in channel 1 is not corrected.

Figures 5a–c show histograms of τ_1^A, τ_2^A, and α, respectively. They give an example of the effect of the correction (using coefficients derived from 1 May 1998 data) on the derived τ_2^A and α for 20 February 1998. The correction reduces τ_2^A (Fig. 5b) by an average of 0.12, shifting the mode of its histogram from $\sim$0.23 down to $\sim$0.11. The most important qualitative feature of the corrected result is that the τ_2^A histogram is now positioned to the left of the τ_1^A histogram, consistent with the observed sun-photometer statistics (e.g., Smirnov et al. 1995). This effect is additionally illustrated by the histogram of the Ångström exponent (Fig. 5c), which shifts its mode from about -0.4 to a positive value of $\sim +0.3$. The average correction $\delta\tau_2^A$ is on the order of the average τ_2^A itself and is about half of the $\mathrm{Max}(\delta\tau_2^A)$ theoretically predicted in section 4a. The modal value, after correction, is substantially lower than the Ångström exponent corresponding to the retrieval model ($\sim$1.25), and it still exhibits a relatively large proportion of negative values. This result suggests, as discussed in section 3, that a different type of aerosol exists in the atmosphere than is assumed in the retrieval model. Our next-generation algorithm will use this information to iterate toward a more accurate retrieval of all parameters. These results will be verified through rigorous comparison with other satellite retrievals and with sun-photometer observations. Some examples of this approach are discussed in the next section with respect to the current-generation algorithm.

5. Consistency checks of retrievals

Some elements of the consistency checks discussed below were proposed in the literature for quality control of ground-based measurements (sun-photometer; Korotaev et al. 1993) and satellite retrievals of sea surface temperature (Ignatov and Gutman 1995) and aerosol (Wagener et al. 1997; Higurashi and Nakajima 1999). This section seeks to formulate a comprehensive set of checks, including the above-mentioned elements, and to apply them for testing real VIRS data. These tests are to be periodically run with the VIRS retrievals, with the

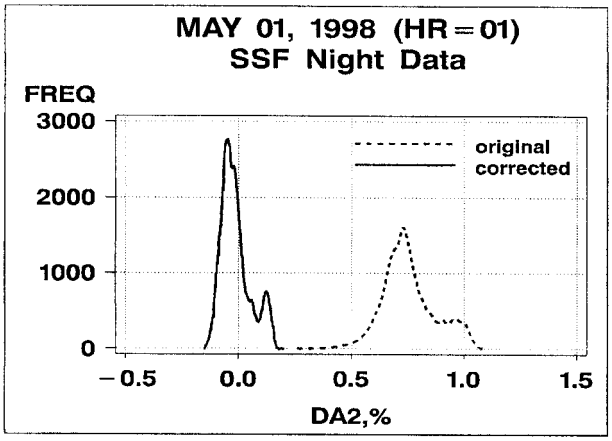

FIG. 4. Frequency distributions of dark albedo for channel 2 (''original''), and its residual error after correction (''corrected'').

[4] Figure 3 may hint at a slightly nonlinear trend in $DA_2(R_4)$. We have tested a quadratic fit in R_4, and found the resulting improvement to be statistically insignificant. Additionally, it is better to avoid any nonlinear terms in radiance, because of the use of VIRS data with different spatial scales. In particular, application of the above coefficients derived from pixel level to the data averaged in space (SSF), or even derivation of the coefficients from space-averaged radiances, may not be straightforward.

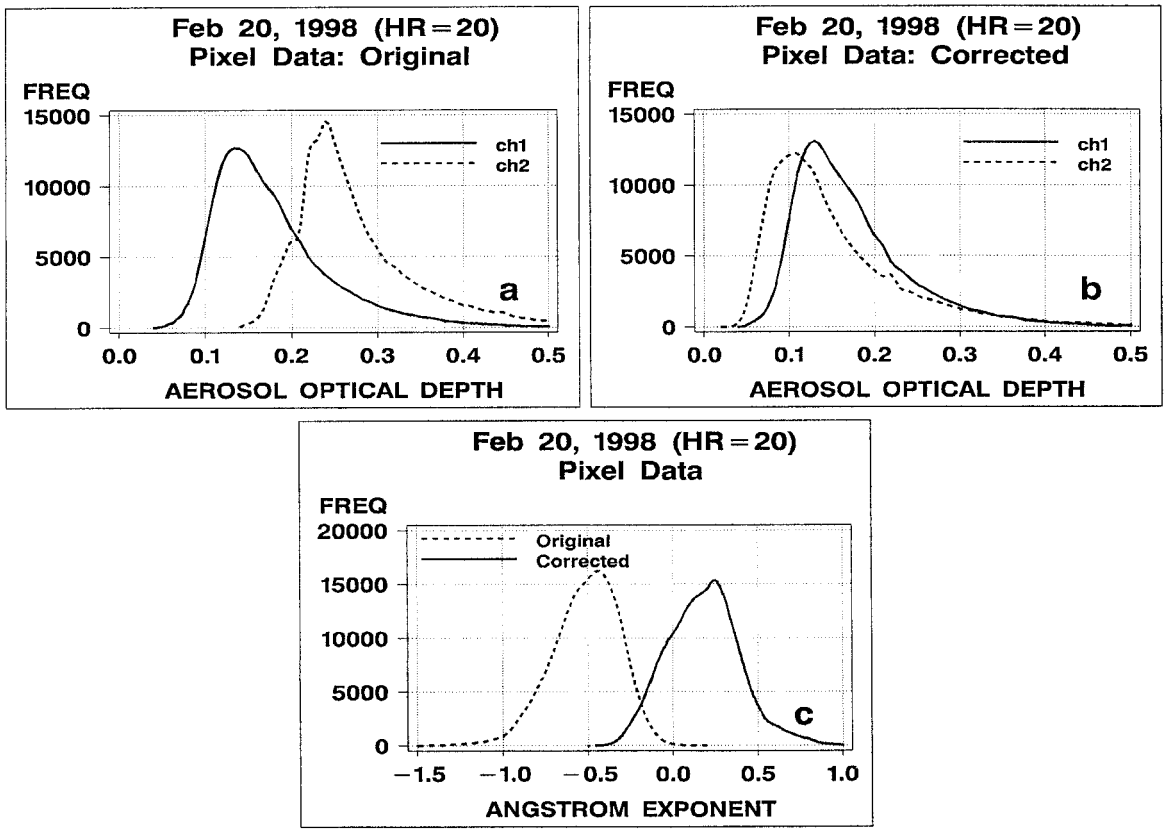

FIG. 5. Frequency distributions of the retrieved τ_1^A, τ_2^A, and α before and after the dark-albedo correction (described in Table 1) for the first day for which dark-albedo data became available, 20 Feb 1998.

objective to uncover and to resolve their most obvious inconsistencies. The ultimate measure of their accuracy can be achieved only through rigorous validation against ground-based sun-photometers and comparisons with other satellite retrievals that are presently underway and whose results will be reported elsewhere.

a. Histograms of τ^A and α

Statistical summaries of sun-photometer observations, available from the scientific literature, provide guidance on the typical values of τ^A and α over the oceans and the expected ranges of their variability (e.g., Smirnov et al. 1995). In particular, τ^A retrievals must be positive and range between $\text{Min}(\tau^A) \sim 0$ (a small percentage of slightly negative retrievals may occur due to noise–digitization–retrieval errors) and $\text{Max}(\tau^A) \sim 1.0$, whereas the Ångström exponent is expected to range between $\text{Min}(\alpha) \sim 0$ and $\text{Max}(\alpha) \sim 2$. The frequency distributions typical of open oceans are expected to peak at ~0.1–0.2 for τ_1^A, ~0.05–0.1 for τ_2^A, and 0.5 ± 0.5 for α, although observations in the spectral interval of channel 2 (1.6 μm) are not abundant and the properties of aerosols at this wavelength are poorly understood at this time.

Figures 6a,b show frequency distributions of τ_1^A, τ_2^A, and α for one orbit of TRMM VIRS data (see Fig. 6e) averaged into the CERES/SSF format for 1 May 1998. It is interesting that the shape of τ^A histograms is close to lognormal [i.e., $\log \tau^A$ is normally distributed—see, e.g., King et al. (1980)]. If the observation of τ^A lognormality holds, then α should be distributed normally, as defined by Eq. (2) (cf. Fig. 6b). The modes of the histograms, found at ~0.13 and 0.10 for τ^As and ~0.3 for α, are close to the expected open-ocean values. Note that, although the modal value of α is the same as it was for the pixel-level analysis of Fig. 5, there is a noticable reduction in the proportion of negative values. This result illustrates the noise-reducing benefits of the space averaging that occurs within the SSF dataset.

b. Scattergram of τ_2^A versus τ_1^A

This test allows one to uncover additive and possibly multiplicative errors in the τ^As. It originally was proposed by Korotaev et al. (1993) for quality control of sun-photometer measurements and is applied here to VIRS retrievals. If τ^As are free of errors, then 1) the scattergram of τ_2^A vs τ_1^A should converge at the origin (i.e., ''no aerosol'' in one channel corresponds to ''no aerosol'' in the other), and 2) the scatter of observations should lie between the lines defining $\alpha \approx 0$ and $\alpha \approx$

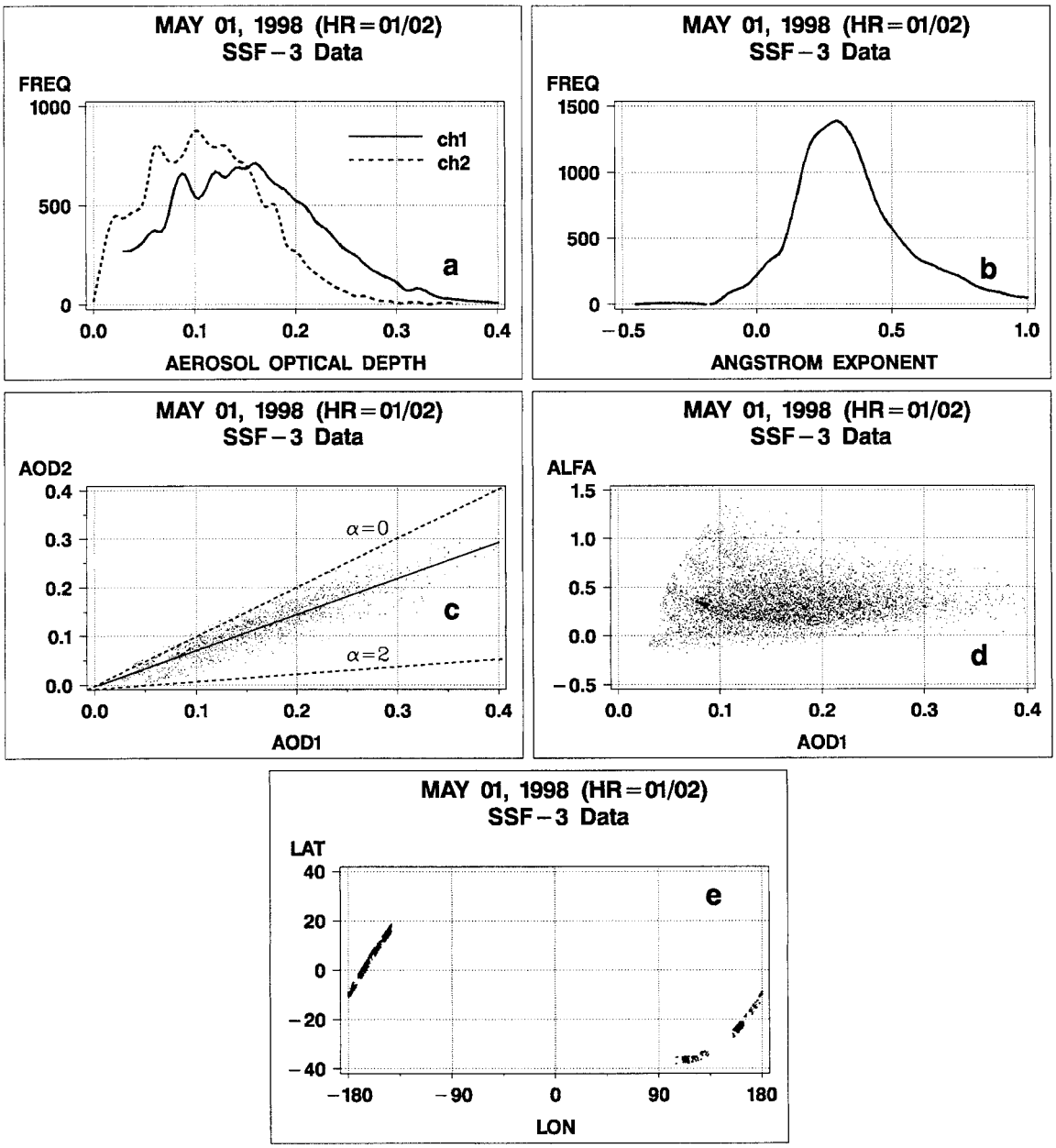

FIG. 6. Consistency checks of τ_1^A, τ_2^A, and α derived from SSF-3 data for 1 May 1998: (a) frequency distributions of τ_1^A and τ_2^A; (b) frequency distribution of α; (c) scattergram of τ_1^A vs τ_2^A; (d) scattergram of α vs τ_1^A; (e) suborbital track of orbit from which data have been analyzed.

2. As shown in Fig. 6c, the observations during this orbit mostly satisfy these expectations. The intercept of a regression line through the observations is less than -0.01, and most observations lie well within the expected values imposed by the Ångström-exponent lines. The scatter should be expected to increase progressively at higher τ^As from the natural variability in the aerosol Ångström-exponent over this orbit. However, errors in one channel with respect to the other are causing a few retrieval points to fall outside of the expected sector.

c. Scattergram of α versus τ_1^A

This check is suggested by the analyses in section 3 of this paper and in Ignatov et al. (1998), which show that the error in the Ångström exponent increases as AOD decreases. Scattergrams of α versus τ_1^A are used to check if α reveals a $1/\tau^A$-type *trend.* If it does, this may be indicative of systematic errors in the τ^A retrievals. A $1/\tau^A$-type *increase in scatter,* symmetrical with respect to the horizontal axis, would be indicative of random errors in the τ^A retrievals.

Figure 6d shows the scattergram for α versus τ_1^A, in which α tends to increase systematically and scatter in α increases as τ_1^A decreases, as expected if both systematic and random errors are present in the AOD values. Figure 6d suggests, in agreement with qualitative conclusions in section 3, that the retrievals of the Ångström exponent become progressively less reliable at lower values of τ^A. Additional averaging in space and/or time beyond what is done for SSF data would perhaps further reduce the scatter, making these retrievals somewhat more reliable. The SSF retrievals seem to stabilize themselves gradually at $\tau^A > 0.2$–0.3, in agreement with quantitative predictions of section 3.

d. Angle trends in τ^A and α

This category of tests is an extension of the methodology proposed by Ignatov and Gutman (1995), who checked whether the retrievals of sea surface temperature reveal residual trends versus view angle, which, if observed, are indicative of retrieval error. Taking into account a different set of retrieval parameters and the specifics of sun-view-dependent radiative transfer in the visible and near-infrared, this check is extended here to test whether both τ^A and α have any pronounced sun-view–scatter–glint-geometry trends. This check is expected to work better over large areas with uniform aerosol [areas removed from continents are expected to be most uniform, because variance in τ^A is lower there (cf. Husar et al. 1997)]. In a preliminary test, a case study with just 2 h of SSF data (the same orbit examined above) was used. Although the desired sampling uniformity was not achieved (see Fig. 6e), it is adequate for an example of this kind of analysis.

Figures 7 and 8 show dependencies of the statistics (minimum, maximum, mean, and standard deviation) of the three retrieved aerosol parameters as they depend upon the four observational/radiative transfer geometrical factors. Dependence upon geometry serves as an ideal test of retrieval performance, because a retrieved parameter should not depend upon geometrical factors. Trends are least pronounced in the view–zenith angle plot but are larger and more variable with other angles. In particular, significant trends start developing at high sun ($\theta_s < 45°$; Fig. 7) and adjacent to glint ($\gamma < 50°$; Fig. 8), suggesting that sun glint at γ angles of 40°–50° may be affecting the retrievals. There are also some nonuniformities in the scattering angle dependencies, which, according to Eq. (4), may indicate problems with the phase function used in the retrievals. The trends in α tend to be much smaller than in τ^As. This difference is most probably due to the canceling of errors in τ^As when taking their ratios, in agreement with theoretical analyses of section 3. Retrievals of τ_1^A may be overestimated by a few hundredths, as indicated by elevated minimum τ_1^As in Figs. 7 and 8. [Note: Recently, a later version of SSF (-4) has been analyzed for ten days in February 1998 for the central Pacific. All of the above conclusions hold, except that the glint angle trends are much less. This result has been attributed to an improved cloud-screening algorithm in SSF-4.]

e. Geographical trends in τ^A and α

Wagener et al. (1997) proposed to plot τ^A retrievals versus latitude and longitude, to check for geographical trends in the retrieved parameters. Thus, VIRS retrievals of both τ^A and α are examined in this way, chiefly to test for regional differences in retrieval errors. Figure 9 shows the statistics (mean, standard deviation, minimum, and maximum) of the three retrieved parameters versus latitude and longitude. As Fig. 5c shows, the ocean areas covered by the 1 May orbit are located well away from dust sources. Even in these remote areas, however, $\tau^A_{\max}$ is unexpectedly low, suggesting that some τ^As may be misclassified as cloud by the SSF-3 cloud-screening algorithm. All others retrieved parameters are well within their expected ranges. The local maximum near 20°S and 160°E–180° may be associated with aerosols originating in Australia.

6. Concluding remarks

Aerosol retrievals from VIRS channels 1 (0.63 μm) and 2 (1.61 μm) are presently made with a remote sensing algorithm that is simple, robust, and consistent with tradition and the level of complexity of the satellite sensor. However, theoretical and empirical examinations of the output from this procedure indicate that worst-case errors can, at times, erode the usefulness of the aerosol product, primarily because of deficiencies of the Dave (1973) RT code, and deviations of the phase function (aerosol model) from that assumed in the retrieval algorithm.

The theoretical error analysis in section 3 has shown that errors in τ^As are subdivided into multiplicative and additive terms. In the case of individual pixel-level retrievals (before spatial and temporal averaging), the worst-case estimates are $\text{Max}(\delta\tau_1^A) \sim \pm 0.35\tau_1^A \pm$ (0.04–0.08) and $\text{Max}(\delta\tau_2^A) \sim \pm 0.35\tau_2^A \pm$ (0.03–0.04) over open oceans, and may reach $\text{Max}(\delta\tau_1^A) \sim \pm 0.35\tau^A \pm$ (0.04–0.08) + (0.03–0.10) and $\text{Max}(\delta\tau_2^A) \sim \pm 0.35\tau_2^A \pm$ (0.03–0.04) + (0.03–0.10) over coastal waters. The fact that the additive errors in channel 2 are even slightly lower than in channel 1 over open oceans does deviate somewhat from the intuitive expectation of greater errors in channel 2, because of the contamination from a thermal leak at 5.2 μm. However, the actual error budget is composed of physical (algorithm related) and instrumental (calibration and thermal leak) components. The expected instrumental errors are comparable in the two channels. (In channel 1, a calibration error of 5% may lead to $\delta\tau_1^A \sim 0.02$, from a Rayleigh-scattering term. The Rayleigh scattering is ~40 times less in channel 2, but the error from the residual of the thermal leak correction in channel 2 is

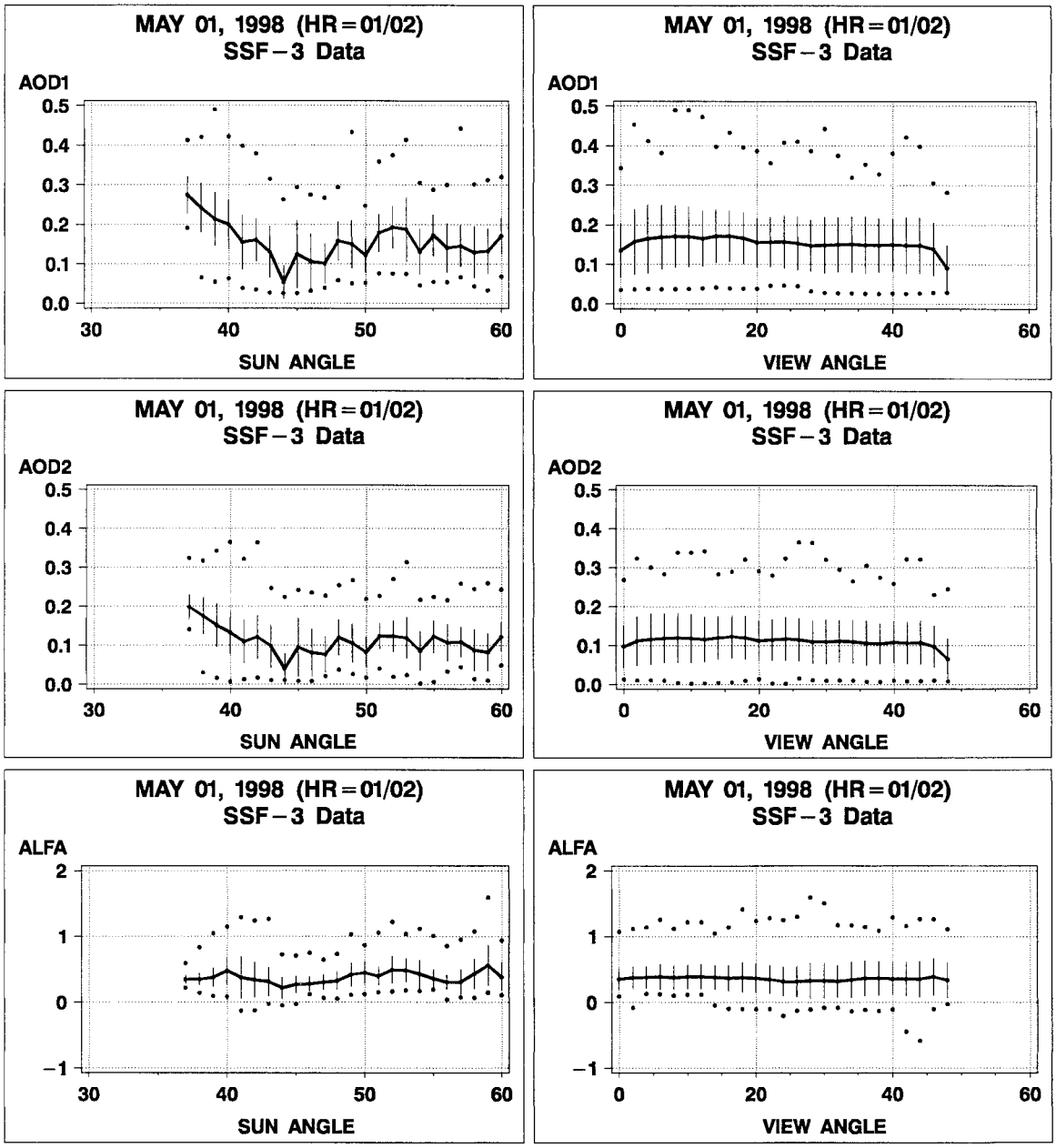

FIG. 7. Statistics of (top) τ_1^A (middle) τ_2^A, and (bottom) α retrievals (mean, standard deviation, minimum, and maximum) versus (left) sun (θ_s) and (right) view (θ_v) zenith angles.

about the same: $\delta\tau_2^A \sim 0.03$.) The algorithm-related errors, however, are much smaller in channel 2, because of a 40-times smaller Rayleigh term and smaller variability in the diffuse surface reflectance (from underlight and foam). Note also that the same additive error in τ^A may be of greater relative effect in channel 2, because of its 30%–40% smaller aerosol optical depth in comparison with channel 1.

Errors in α vary in inverse proportion to τ^A. When $\tau_1^A > 0.15$–0.30 and $\tau_2^A > 0.10$–0.15, then $\text{Max}(\delta\alpha) < \pm 0.5$. Some errors in τ^As and α are always systematic (e.g., those from calibration uncertainties), and some may be systematic or random, depending upon the space scales and timescales upon which the retrievals are based (oceanic reflectance, aerosol model, and Rayleigh optical depth). Under typical conditions, and after averaging, worst-case random errors should be significantly reduced. Several empirical examples of this reduction have been presented.

Before retrieving τ_2^A, the reflectance in channel 2

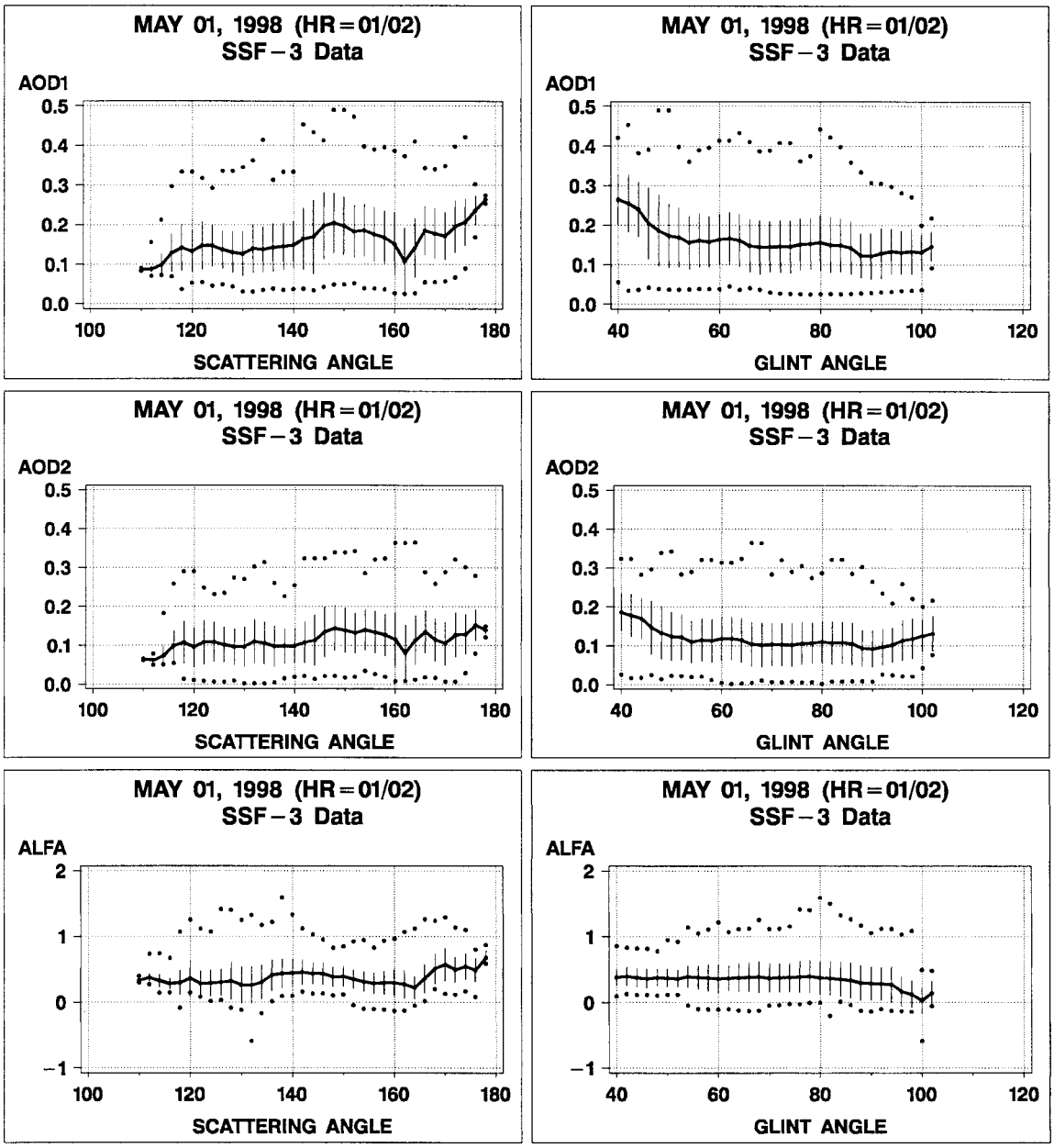

FIG. 8. Same as in Fig. 7 but versus (left) scattering (χ) and (right) glint (γ) angles. (The γ is defined as angle away from glint direction: $\gamma = 0°$ when satellite views exactly toward glint.)

needs to be corrected for a leak of thermal radiation that results from an inadvertent secondary spectral response peak near $\sim$5.2 μm. The parameterizations of the thermal leak are derived empirically using nighttime measurements and are applied to the daytime reflectance measurements. After correction, the maximum (worst case) errors in τ_2^A from residual thermal leak effects are expected to range between $\pm$0.015 and $\pm$0.030, depending upon geometry (equivalent to $\sim\pm$0.005–0.010 root-mean-square errors). Without correction, the error in τ_2^A ranges between +0.12 and +0.25, which is unacceptably large.

A comprehensive set of consistency checks also has been formulated and applied to the retrievals. These quality-control and consistency checks are currently used to evaluate the performance of the current algorithm and to assist in developing the next-generation algorithm. Preliminary results suggest that the retrievals are, to a large extent, self- and interconsistent, although some artificial trends in solar zenith, glint, and scattering

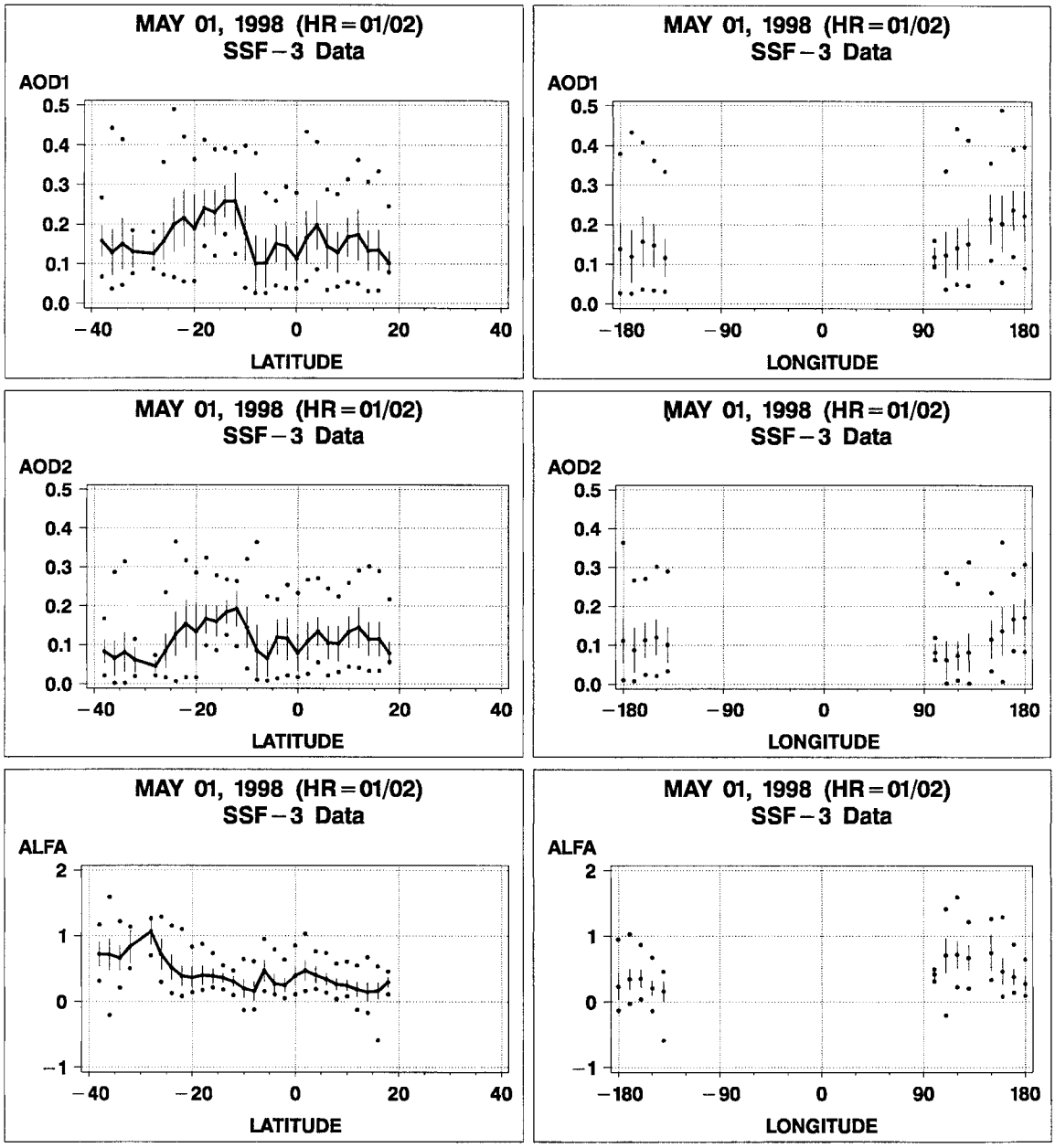

FIG. 9. Same as in Fig. 7 but versus (left) latitude and (right) longitude.

angle are present. Retrievals of τ_1^A may be overestimated by a few hundredths (cf. elevated minimum τ_1^As in Figs. 7 and 8), and the assumed phase function may be biased (cf. the scatter-angle trends in Fig. 8). Self-consistency checks are being applied to other days from the available TRMM/CERES VIRS data record, to ensure the suitability of the derived aerosol parameters for the climate studies for which they are intended. The ultimate way of evaluating the product is its validation against ground-based sun-photometers and comparison with other satellite retrievals (e.g., AVHRR). This effort is presently underway, and its results will be reported elsewhere.

Acknowledgments. VIRS pixel data were provided by Pat Minnis's group at the NASA LaRC, in particular, by Sunny Sun-Mack; CERES-SSF data were provided by Erika Geier and Linda Hunt at the NASA LaRC Data Active Archive Center (DAAC). At different stages of this work, we received help from Sunny Sun-Mack, Tim Murray, David Kratz, and Walt Miller of NASA LaRC. While working on the problem of the

thermal-leak correction, we have been helped by NASA LaRC and advised by Bill Barnes, Chris Kummerow, and Chen-Hsuan Lyu of NASA GSFC. This study was supported by NASA Contract L-90987C. We thank Bruce Wielicki and Bruce Barkstrom for support and encouragement. We greatly acknowledge very constructive and useful comments by reviewers and the editor, which led to major revision of the first draft of the paper.

APPENDIX

Radiometric Definitions Used in the Paper

- L_i (W m^{-2} sr^{-1}): Radiance in VIRS channel i (i = 1, 2); (reflected component).
- F_i (W m^{-2} sr^{-1}): Effective solar (perfect Lambert reflector) radiance in VIRS channel i (i = 1, 2); F_1 = 537.1, F_2 = 78.0 W m^{-2} sr^{-1}.
- $A_i = L_i/F_i$ (dimensionless), or $A_i = 100L_i/F_i$ (%): Normal incident (or overhead sun) albedo in VIRS channel i (i = 1, 2; reflected component). Lookup tables used in the retrievals are expressed in albedo units, consistent with the NOAA operational tradition.
- $\rho_i = L_i/(F_i\mu_s)$ (dimensionless), or $\rho_i = 100L_i/(F_i\mu_s)$ (%): Reflectance factor in VIRS channel i (i = 1, 2). Related to the normal incident albedo as $\rho = A/\mu_s$.
- R_i (W m^{-2} μm^{-1} sr^{-1}): Radiance in VIRS channel i (i = 1–5; thermal component only).
- $\mathrm{DA}_i = R_i/F_i$ (dimensionless), or $\mathrm{DA}_i = 100R_i/F_i$ (%): Thermal component of the normal incident (overhead sun) dark albedo in VIRS channel i (i =1, 2; normalization to ''overhead'' sun is made for daytime and nighttime measurements, for consistency).
- λ_i: Central wavelength of channel i (λ_1 = 0.63, λ_2 = 1.536, λ_3 = 3.7, λ_4 = 10.8, and λ_5 = 11.0 μm).
- τ_i^A: AOD in channel i (i = 1, 2).
- $\alpha = -\ln(\tau_1^A/\tau_2^A)/\ln(\lambda_1/\lambda_2)$: Ångström exponent.
- $\Lambda = -1/\ln(\lambda_1/\lambda_2) \sim 1.1$: Spectral separation factor of the channels.
- ω_i: Aerosol SSA in channel i (i = 1, 2).
- $P_i^A(\chi)$: Aerosol phase function in channel i (i = 1, 2); χ is scattering angle.

REFERENCES

Ångström, A., 1961: Techniques of determining the turbidity of the atmosphere. *Tellus,* **XIII,** 214–223.

——, 1964: The parameters of atmospheric turbidity. *Tellus,* **XVI,** 214–223.

Barnes, R. A., W. L. Barnes, C.-H. Lyu, and J. M. Gales, 2000: An overview of the visible and infrared scanner radiometric calibration algorithm. *J. Atmos. Oceanic Technol.,* **17,** 395–405.

Charlson, R. J., S. E. Schwartz, J. M. Hales, R. D. Cess, J. A. Coakley Jr., J. E. Hansen, and D. J. Hofmann, 1992: Climate forcing by anthropogenic aerosols. *Science,* **255,** 423–430.

d'Almeida, G. A., P. Koepke, and E. P. Shettle, 1991: *Atmospheric Aerosols, Global Climatology and Radiative Characteristics.* A.Deepak Publishing, 561 pp.

Dave, J. V., 1973: Development of the programs for computing characteristics of ultraviolet radiation: Scalar case. Tech. Rep. NAS5-21680, NASA GSFC, Greenbelt, MD, 130 pp.

Durkee, P. A., F. Pfeil, E. Frost, and E. Shima, 1991: Global analysis of aerosol particles characteristics. *Atmos. Environ.,* **25A,** 2457–2471; *Science,* **255,** 423–430.

——, and Coauthors, 2000: Regional aerosol optical depth characteristics from satellite observations: ACE-1, TARFOX and ACE-2 results. *Tellus,* in press.

Frouin, R., M. Schwindling, and P.-Y. Deschamps, 1996: Spectral reflectance of sea foam in the visible and near-infrared: In situ measurements and remote sensing applications. *J. Geophys. Res.,* **101,** 14 361–14 371.

Geogdzhaeyev, I. V., and M. I. Mischenko, 1999: Sensitivity analysis of aerosol retrieval algorithms using two-channel satellite radiance data. *Proc. SPIE,* **3763,** 1–13.

Gordon, H. R., and A. Y. Morel, 1983: *Remote Assessment of Ocean Color for Interpretation of Satellite Visible Imagery: A Review.* Springer Verlag, 114 pp.

Higurashi, A., and T. Nakajima, 1999: Development of a two-channel aerosol retrieval algorithm on a global scale using NOAA AVHRR. *J. Atmos. Sci.,* **56,** 924–941.

Husar, R., J. Prospero, and L. L. Stowe, 1997: Characterization of tropospheric aerosols over the oceans with the NOAA/AVHRR optical thickness operational product. *J. Geophys. Res.,* **102,** 16 889–16 910.

Ignatov, A., and G. Gutman, 1995: The empirical angular function approach: Testing sea surface temperature retrievals. *J. Appl. Meteor.,* **34,** 2091–2097.

——, L. Stowe, S. Sakerin, and G. Korotaev, 1995a: Validation of the NOAA/NESDIS satellite aerosol product over North Atlantic in 1989. *J. Geophys. Res.,* **100,** 5123–5132.

——, ——, R. Singh, S. Sakerin, D. Kabanov, and I. Dergileva, 1995b: Validation of NOAA/AVHRR aerosol retrievals using sun-photometer measurements from RV *Akademik Vernadsky* in 1991. *Adv. Space Res.,* **16,** 95–98.

——, ——, and ——, 1998: Sensitivity study of the Ångström exponent derived from AVHRR over the oceans. *Adv. Space Res.,* **21,** 439–442.

Kaufman, Y., 1993: Aerosol optical thickness and atmospheric path radiance. *J. Geophys. Res.,* **98,** 2677–2692.

——, and Coauthors, 1997: Passive remote sensing of tropospheric aerosol and atmospheric correction for the aerosol effect. *J. Geophys. Res.,* **102,** 16 815–16 830.

Kidwell, K., 1995: NOAA polar orbiter data users guide. NOAA/NESDIS, 192 pp.

King, M., D. M. Byrne, J. A. Reagan, and B. M. Herman, 1980: Spectral Variation of aerosol optical depth at Tucson, Arizona, between August 1975 and December 1977. *J. Appl. Meteor.,* **19,** 723–732.

Korotaev, G., S. Sakerin, A. Ignatov, L. Stowe, and P. McClain, 1993: Sun-photometer observations of aerosol optical depth over the North Atlantic from a Soviet research vessel for validation of satellite measurements. *J. Atmos. Oceanic Technol.,* **10,** 725–735.

Lacis, A. A., and M. I. Mishchenko, 1995: Climate forcing, climate sensitivity, and climate response: A radiative modeling perspective on atmospheric aerosols. *Aerosol Forcing of Climate,* R. T. Charlson and J. Heintzenberg, Eds., John Wiley and Sons, 11–42.

Lyu, C.-H., W. L. Barnes, and R. A. Barnes, 2000: First results from the on-orbit calibrations of the visible and infrared scanner for the Tropical Rainfall Measuring Mission. *J. Atmos. Oceanic Technol.,* **17,** 385–394.

McClain, E. P., W. G. Pichel, and C. Walton, 1985: Comparative performance of AVHRR-based multichannel sea surface temperatures. *J. Geophys. Res.,* **90,** 11 587–11 601.

Mishchenko, M. I., I. V. Geogdzhayev, B. Cairns, W. B. Rossow, and A. Lacis, 1999: Aerosol retrievals over the oceans by use of

channels 1 and 2 AVHRR data: Sensitivity analysis and preliminary results. *Appl. Opt.,* **38,** 7325–7341.

Nakajima, T., and A. Higurashi, 1997: AVHRR remote sensing of aerosol optical properties in the Persian Gulf region, summer 1991. *J. Geophys. Res.,* **102,** 16 935–16 946.

Quenzel, H., and M. Kaestner, 1980: Optical properties of the atmosphere: Calculated variability and application to satellite remote sensing of phytoplankton. *Appl. Opt.,* **19,** 1338–1344.

Royer, A., N. O'Neill, A. Davis, and L. Huebert, 1988: Comparison of radiative transfer models used to determine atmospheric optical parameters from space. *Proc. SPIE,* **928,** 118–135.

Shettle, E. P., and R. W. Fenn, 1979: Models for the aerosols of the lower atmosphere and the effects of humidity variations on their optical properties. Environmental Research Paper 675, AFGL-TR-79-0214, 94 pp.

Smirnov, A., O. Yershov, and Yu. Villevalde, 1995: Measurements of aerosol optical depth in the Atlantic Ocean and Mediterranean Sea. *Proc. SPIE,* **2582,** 203–214.

Stowe, L. L., A. Ignatov, and R. Singh, 1997: Development, validation and potential enhancements to the second generation operational aerosol product at NOAA/NESDIS. *J. Geophys. Res.,* **102,** 16 923–16 934.

Tanre, D., Y. J. Kaufman, M. Herman, and S. Matoo, 1997: Remote sensing of aerosol properties over oceans using the MODIS/EOS spectral radiances. *J. Geophys. Res.,* **102,** 16 971–16 988.

Vermote, E., D. Tanre, J. L. Deuze, M. Herman, and J. J. Morcrette, 1997: Second simulation of the satellite signal in the solar spectrum, ''6S'': An overview. *IEEE Trans. Geosci. Remote Sens.,* **35,** 675–686.

Viollier, M., D. Tanre, and P. Y. Deshamps, 1980: An algorithm for remote sensing of water color from space. *Bound.-Layer Meteor.,* **18,** 247–267.

Wagener, R., S. Nemesure, and S. E. Schwartz, 1997: Aerosol optical depth over oceans: High space- and time-resolution retrieval and error budget from satellite radiometry. *J. Atmos. Oceanic Technol.,* **14,** 577–590.

Wielicki, B. A., B. R. Barkstrom, E. F. Harrison, R. B. Lee III, G. L. Smith, and J. E. Cooper, 1996: Clouds and the Earth's Radiant Energy System (CERES): An Earth Observing System experiment. *Bull. Amer. Meteor. Soc.,* **77,** 853–868.